ENEA
AGENZIA NAZIONALE PER LE NUOVE TECNOLOGIE,
L'ENERGIA E LO SVILUPPO ECONOMICO SOSTENIBILE

ISSN/0393-3016

GROWTH AND CHARACTERISATION OF THERMALLY-EVAPORATED LITHIUM FLUORIDE THIN FILMS FOR HIGH-ENERGY RADIATION DETECTORS

M.A. VINCENTI, R.M. MONTEREALI
ENEA - Unità Tecnica Sviluppo di Applicazione delle Radiazioni
Laboratorio Micro e Nano Strutture per la Fotonica
Centro Ricerche Frascati, Roma

G. MESSINA
ENEA - Unità Tecnica Sviluppo di Applicazione delle Radiazioni
Laboratorio Sorgenti di Radiazione
Centro Ricerche Frascati, Roma

E. NICHELATTI
ENEA - Unità Tecnica Tecnologie dei Materiali
Laboratorio Sviluppo e Realizzazione di Componenti Ottici
Centro Ricerche Casaccia, Roma

A. MANCINI, A. RUFOLONI
ENEA – Unità Tecnica Fusione
Laboratorio di Superconduttività
Centro Ricerche Frascati, Roma

RT/2013/22/ENEA

AGENZIA NAZIONALE PER LE NUOVE TECNOLOGIE,
L'ENERGIA E LO SVILUPPO ECONOMICO SOSTENIBILE

GROWTH AND CHARACTERISATION OF THERMALLY-EVAPORATED LITHIUM FLUORIDE THIN FILMS FOR HIGH-ENERGY RADIATION DETECTORS

M.A. VINCENTI, R.M. MONTEREALI

ENEA - Unità Tecnica Sviluppo di Applicazione delle Radiazioni
Laboratorio Micro e Nano Strutture per la Fotonica
Centro Ricerche Frascati, Roma

G. MESSINA

ENEA - Unità Tecnica Sviluppo di Applicazione delle Radiazioni
Laboratorio Sorgenti di Radiazione
Centro Ricerche Frascati, Roma

E. NICHELATTI

ENEA - Unità Tecnica Tecnologie dei Materiali
Laboratorio Sviluppo e Realizzazione di Componenti Ottici
Centro Ricerche Casaccia, Roma

A. MANCINI, A. RUFOLONI

ENEA – Unità Tecnica Fusione
Laboratorio di Superconduttività
Centro Ricerche Frascati, Roma

RT/2013/22/ENEA

I Rapporti tecnici sono scaricabili in formato pdf dal sito web ENEA alla pagina
http://www.enea.it/it/produzione-scientifica/rapporti-tecnici

I contenuti tecnico-scientifici dei rapporti tecnici dell'ENEA rispecchiano l'opinione degli autori e non necessariamente quella dell'Agenzia.

The technical and scientific contents of these reports express the opinion of the authors but not necessarily the opinion of ENEA.

GROWTH AND CHARACTERISATION OF THERMALLY-EVAPORATED LITHIUM FLUORIDE THIN FILMS FOR HIGH-ENERGY RADIATION DETECTORS

M.A. VINCENTI, R. M. MONTEREALI, G. MESSINA, E. NICHELATTI, A. MANCINI, A. RUFOLONI

Abstract
Lithium fluoride (LiF) polycrystalline thin films grown on glass substrates by thermal evaporation were characterised by means of Atomic Force Microscopy (AFM), Scanning Electron Microscopy (SEM), optical transmittance and reflectance spectra and X-Ray Diffraction (XRD). A theoretical model was used to evaluate from measured photometric spectra some properties of the coating, such as film thickness, superficial roughness, material inhomogeneity along the growth axis, etc.. Optical absorption, photoluminescence and photo-excitation spectra of LiF thin films of increasing thicknesses were measured before and after irradiation with a 5 MeV electron beam. The Combined Excitation-Emission Spectroscopy (CEES) technique was successfully applied to investigate the kind of colour centres produced in these thin films by beta irradiation. Luminescent LiF thin films are currently under study as novel and versatile imaging detectors of high-energy radiation beams and other radiation sources.

Key words: *LiF, thin films, AFM, transmittance, photoluminescence, photoluminescence-excitation, CEES*

CRESCITA E CARATTERIZZAZIONE DI FILM SOTTILI DI FLUORURO DI LITIO DEPOSITATI PER EVAPORAZIONE TERMICA PER RIVELATORI DI RADIAZIONE DI ALTA ENERGIA

Riassunto
Film sottili policristallini di fluoruro di litio (LiF) depositati per evaporazione termica su substrati di vetro sono stati caratterizzati mediante Microscopia a Forza Atomica (AFM), Microscopia Elettronica a Scansione (SEM), spettri di trasmittanza e riflettanza ottica e Diffrazione a Raggi X (XRD). E' stato utilizzato un modello teorico per valutare da misure spettrofotometriche alcune proprietà dello strato depositato, come lo spessore del film, la rugosità superficiale, la disomogeneità del materiale lungo l'asse di crescita, ecc.. Gli spettri di assorbimento ottico, di fotoluminescenza e di fotoeccitazione dei film sottili di LiF di diverso spessore sono stati misurati prima e dopo l'irraggiamento con un fascio di elettroni da 5 MeV. La tecnica di Spettroscopia Combinata di Eccitazione-Emissione (CEES) è stata applicata con successo per studiare il tipo di centri di colore prodotti dall'irraggiamento beta in questi film. Film sottili luminescenti di LiF sono attualmente oggetto di studio come rivelatori a lettura ottica, innovativi e versatili, di fasci di radiazione ad alta energia e di altre sorgenti di radiazione ionizzante.

Parole chiave: LiF, film sottili, AFM, trasmittanza, fotoluminescenza, foto eccitazione, CEES

INDEX

1. INTRODUCTION……………………………………………………………………....7
2. LITHIUM FLUORIDE AND COLOUR CENTRES……………………………………..….8
3. LiF THIN FILMS GROWN BY THERMAL EVAPORATION…………………………...11
4. GP20 DEPOSITION SYSTEM…………………………………………………….…….12
5. ATOMIC FORCE MICROSCOPY AND SCANNING ELECTRON MICROSCOPY INVESTIGATION OF LiF THIN FILMS……………………………………………….14
6. SPECTROPHOTOMETRIC CHARACTERISATION OF LiF THIN FILMS....................16
7. X-RAY DIFFRACTION OF LiF THIN FILMS……………..……………………….….19
8. OPTICAL AND SPECTROSCOPIC CHARACTERISATION OF LiF THIN FILMS IRRADIATED BY HIGH-ENERGY ELECTRONS…………………….…………....20
   - 8.1 Optical absorption measurements of beta-irradiated LiF thin films…………………....20
   - 8.2 Photoluminescence and photoluminescence-excitation measurements of beta-irradiated LiF thin films grown on glass substrates……………………………………………22
   - 8.3 Combined Excitation-Emission Spectroscopy...25

CONCLUSIONS………………………………………………………….………...….27

REFERENCES...28

GROWTH AND CHARACTERISATION OF THERMALLY-EVAPORATED LITHIUM FLUORIDE THIN FILMS FOR HIGH-ENERGY RADIATION DETECTORS

1. INTRODUCTION

Nowadays there is a great interest in the technological research about luminescent materials for development of solid state detectors for ionising radiations. They found application in the characterisation of intense ionising radiation sources, decommissioning and storage of radioactive waste, mapping the flux in the out-of-core regions of fission and fusion reactors, but also in scientific imaging applications like new materials investigation, microdevice development and life-science, for X-ray microscopy of biological samples, even for *in vivo* specimens.

The optical and chemical-physical properties of lithium fluoride, LiF, and its sensitivity to ionising radiation (X-rays, gamma-rays, electrons, neutrons etc.) make this material, in pure and doped form, very interesting for several applications in the fields of dosimetry and radiation imaging.

LiF-based radiation imaging detectors assure great versatility, as they can be grown in the form of optically transparent thin films on various substrates by thermal evaporation, tailoring their geometry, size and thickness. The main deposition conditions, such as nature of the substrate, substrate temperature, deposition rate, total thickness, etc., influence the structural, morphological and optical properties of LiF thin films and the formation efficiency of the radiation-induced colour centres.

These novel detectors are characterised by a non-destructive and efficient reading technique based on the optical detection of the visible photoluminescence signal emitted by F_2 and F_3^+ colour centres (stable at room temperature), which are locally produced by irradiation with ionising radiation. Their spatial resolution, intrinsically very high, because comparable with the point

defects size, which is at atomic scale, is limited in the reading process by the characteristics of the optical microscope and the technique utilised for the photoluminescence detection.

In this work the characterisation of thermally-evaporated LiF thin films, grown on glass substrates, by means of Atomic Force Microscopy (AFM), Scanning Electron Microscopy (SEM) and X-Ray Diffraction (XRD) is presented. A theoretical model is introduced to take into account some properties of the LiF coating, such as the film thickness, the superficial roughness and the material inhomogeneity along the growth axis. The optical and spectroscopic characterisation of LiF thin films is performed before and after the irradiation with 5 MeV electrons. An advanced spectroscopic technique, called Combined Excitation-Emission Spectroscopy (CEES), is applied to investigate the kind of colour centres (CCs) produced in LiF films by beta irradiation.

2. LITHIUM FLUORIDE AND COLOUR CENTRES

Among alkali halides (AH) and other dielectric materials, LiF occupies a special place because of its peculiar chemical-physical and optical properties. LiF consists of two interpenetrating fcc lattices, one for Li^+ ions and one for F^- ions. LiF crystals are hard and almost not hygroscopic [1], two precious properties for optical materials. The nearest-neighbour distance, 0.2013 nm, is the shortest among AH; the Li^+ cation and the F^- anion have the smallest radius among the alkali and halide ions, 0.06 nm and 0.136 nm, respectively. The melting point of LiF, 848.2 °C, is lower than the expected values for the series of alkali fluorides. LiF has got a band gap greater than 14 eV [2], so it is optically transparent from 120 nm to 7 µm (from ultraviolet, UV, to infrared, IR) and for this reason it is a widely used window material, in particular in the UV. Its refractive index, 1.3912 at 640 nm and room temperature (RT) [3], is among the lowest ones of solid dielectric materials. Table 1 reports the main physical parameters of LiF.

Table 1. Main physical parameters of LiF.

Nearest neighbour distance (Å)	2.013
Melting point (°C)	848.2
Density (g/cm^3 at RT)	2.639
Molecular weight	25.939
Refractive index at 640 nm, RT	1.3912
Solubility (g/100 g H_2O at 25 °C)	0.134
Knoop Hardness (kg/mm^2)	100

LiF is a very promising radiation-sensitive material, which is widely used in radiation dosimetry [4, 5], optoelectronics [6] and integrated optics [7]. It has also been deeply studied as far as basic optical properties of CCs are concerned [8]. In dosimetry applications LiF can be doped with

special impurities (LiF:Mg,Ti, LiF:Mg,Cu,P) to enhance its sensitivity to ionising radiations and/or to obtain the near tissue-equivalence of the material [9].

Pure and doped AH, containing CCs, were studied carefully because they were considered as prototypes of other kinds of defects in more complex insulating materials. Contrary to the other AH, the usual techniques of additive colouration are not effective in the formation of electronic defects in LiF. LiF can be coloured by several types of ionising radiation (X-rays, gamma-rays, electrons, protons, neutrons, α particles and heavier charged ions). Each radiation source gives rise to different kinds of damaging processes according to the involved particle and its energy. Gamma-rays have a high penetration length and they lose their energy through the material along a thickness of some millimetres, uniformly. Low-energy electron beams (some keV) produce an intense surface colouration, while electron beams with energies of few MeV induce a uniform colouration along thickness of some millimetres. Protons, α particles and ion beams can produce intense surface colourations. For X-rays, the penetration in LiF ranges from few tens of nanometres to several hundreds of micrometers [10, 11] depending on energy.

The primary mechanism of damage by ionising radiation in LiF is radiolysis [12], which is the creation of Frenkel pairs via non-radiative Self Trapped Exciton (STE) decay [8]. The kinetic of colouration is complex and strongly dependent on a large number of variables: the type of ionising radiation and its characteristics, the irradiation conditions, chemical purity, mechanical and thermal history, radiation intensity (dose-rate), temperature etc. All of them influence the level of colouration and the kinds of induced CCs [13].

Primary and aggregate CCs produced in LiF by ionising radiation are stable at RT and give rise to absorption bands that extend from the UV through the visible (Vis) up to Near IR (NIR) region of electromagnetic (e.m.) spectrum. Several of them, if properly excited with e.m. radiation, emit photoluminescence (PL) bands in the Vis and NIR spectral regions [14]. Table 2 reports a list of the main electronic defects in coloured LiF crystals and typical values of the peak position (E_a, E_e) and of the full width at the half maximum ($FWHM_a$, $FWHM_e$) of their absorption and emission bands, respectively, at RT.

The primary colour centre is the F centre, which consists of an anionic vacancy occupied by an electron. Its absorption band is located at about 248 nm [15]. Up to now, the PL originating from the F centre in LiF has not been detected unambiguosly, but a weak emission is theoretically expected at about 900 nm [16, 17]. The F centre plays a crucial role as primary defect which can aggregate to form complexes. As shown in Fig. 1, the aggregate F_2 electronic defect consists of two nearest-neighbour F centres along the <100> direction of the cubic lattice, while the F_3 colour centre consists of three F centres in nearest-neighbour sites in the (111) plane.

F_2 and F_3^+ electronic defects (two electrons bound to two and three anion vacancies, respectively) [18] possess almost overlapping absorption bands, peaked at about 450 nm, generally called M band [19]. Under optical pumping in this spectral region, they emit broad PL bands peaked at 678 nm and 541 nm for F_2 and F_3^+ CCs, respectively (see Table 2), which are only partially overlapped because of a different Stokes shift.

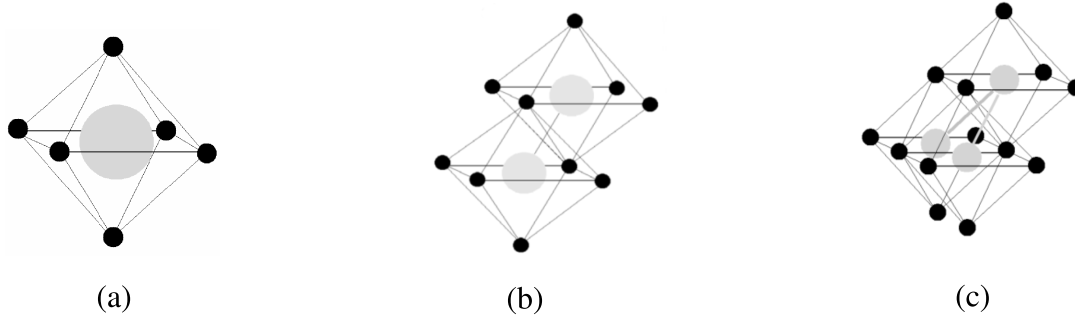

Figure 1. Structure of some colour centres: F (a), F_2 (b) and F_3 (c).

Table 2. Spectroscopic parameters of colour centres in LiF at RT. E_a and $FWHM_a$ are peak position and full width at the half maximum of the absorption band; E_e and $FWHM_e$ are peak position and full width at the half maximum of the emission band. [a]Ref. [15], [b]Ref. [17], [c]Ref. [6], [d]Ref. [20], [e]Ref. [21], [f]Ref. [19] ,[g]Ref.[22].

Centre	E_a (eV) λ_a (nm)	$FWHM_a$ (eV)	E_e (eV) λ_e (nm)	$FWHM_e$ (eV)
F	5.00[a] 248	0.76[a]		
F_2	2.79[b] 444	0.16[b]	1.83[b] 678	0.36[b]
F_3^+	2.77[b] 448	0.29[b]	2.29[b] 541	0.31[b]
F_2^+	1.92[c] 645	0.433[c]	1.36[c] 912	0.29[c]
F_2^-	1.29[c] 960	0.21[c]	1.11[c] 1117	0.17[c]
$F_3(R_1)$	3.92[d] 316	0.52[e]	1.94[d] 640	
$F_3(R_2)$	3.31[d] 374	0.66[e]	2.34[d] 530	
$F_3^-(R_1^{'})$	1.88[d] 660			
$F_3^-(R_2^{'})$	1.55[d] 880	0.190[d]	1.38[d] 898	0.331[d]
$F_4(N_1)$	2.40[f] 517	0.21[e]		
$F_4(N_2)$	2.26[f] 549	0.22[e]		
F_4 – *like*	1.91[g] 648	0.19[g]	1.69[g] 735	0.16[g]

The absorption bands peaked at 316 nm and 374 nm are due to the R_1 and R_2 transitions of F_3 electronic defects [20]. Moreover the absorption bands peaked at 517 nm and 549 nm are attributed to the N_1 and N_2 transitions of the F_4 defects, which consist of four associated F centres [18].

One of the crucial problems concerning irradiated LiF crystals and films is the coexistence of several kinds of aggregate defects with often overlapping absorption bands, which makes it difficult to clearly individuate and measure the single partial contributions due to the individual electronic defects. An accurate determination of the spectroscopic parameters of absorption and emission bands of F_2 and F_3^+ defects was possible from absorption and photoluminescence measurements on suitably treated gamma-coloured LiF crystals, which contain mainly one of these CCs [23] at low volume concentrations.

3. LiF THIN FILMS GROWN BY THERMAL EVAPORATION

LiF thin films can be grown only by physical deposition methods, such as thermal evaporation [24], e-beam evaporation [25] and pulsed laser deposition [26]. As a matter of fact, the ionic nature of AH seems to be not easily compatible with more sophisticated film deposition processes.

Thin films exhibit a wide variety of microstructures, characterised in terms of grain size and crystallographic orientation, lattice defects and surface morphology. Extensive studies of the correlation between film structure and deposition parameters have led to development of the Structure Zone Model (SZM), which categorizes the structural evolution during Physical Vapour Deposition (PVD) as a function of film growth parameters [27, 28].

Structural, morphological and optical properties of a thin film strongly depend on the main depositions parameters such as:

- pressure and nature of residual gas in the deposition chamber;
- temperature of the evaporation source;
- deposition rate of condensing atoms or molecules;
- substrate temperature;
- surface mobility of deposit atoms or molecules on substrate;
- nature of the substrate (amorphous, polycrystalline or mono-crystalline, etc.);
- occurrence of chemical reactions between deposit and substrate;
- total thickness;
- evaporation geometry.

The dependence of the structure and the properties of thin films on the state of the substrate surface is expected for film of average thickness corresponding to only a few atomic diameters, but sometimes the influence of the substrate makes itself felt in thicker films. Moreover, the choice of an orientated substrate plays a dominant role in the determination of the properties of films.

As a result of the standard deposition conditions and of the surface structure of substrates, thin films are generally polycrystalline, i.e. consist of many single monocrystals known as *grains* or *crystallites*. Each grain possesses a neat internal ordering, terminating at the grain boundary, but its orientation is usually completely random with respect to all its neighbours. Typically thin films grown on substrates at or above RT have a grain size of ~100 nm [29, 30]. The structure of polycrystalline thin films has significant influence upon their performance in almost all applications. Porosity, grain shape, grain (or crystallite) size, grain size distributions, grain boundary and grain orientations influence the film properties and stability.

Figure 2 shows, schematically, the operating principle of a thermal evaporation system.

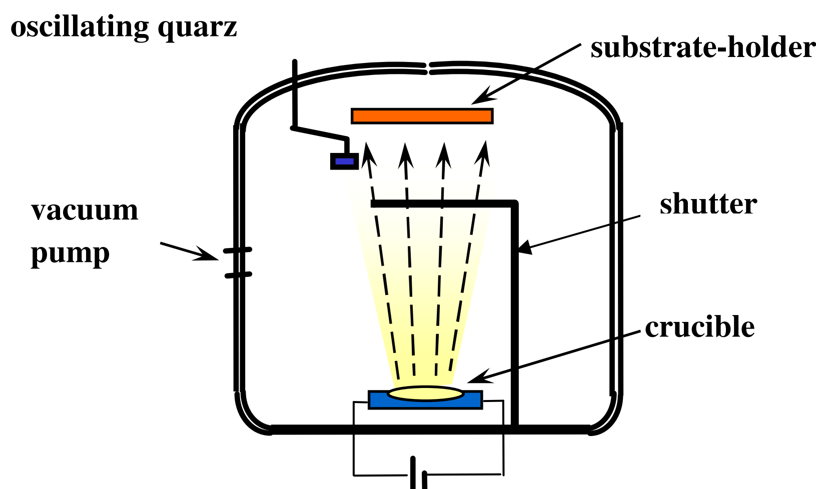

Figure 2. Operating principle of a thermal evaporation system.

4. GP20 DEPOSITION SYSTEM

The GP20 deposition system of SISTEC-Angelantoni S.p.A. (Massa Martana, PG) was used to grow LiF thin films at the Photonic Micro and Nanostructures Laboratory (UTAPRAD-MNF) of ENEA C.R. Frascati. This deposition system essentially consists of a cylindrical steel process chamber provided with several standard lateral CF flanges for visual inspection and for installation of different sensors for diagnostics as vacuum gauges and thermocouples. The geometry of the rotating substrate-holder allows to accommodate up to thirty substrates, which can be amorphous (glass, silica, aluminum on glass, Indium Tin Oxide on glass, plastic) or crystalline (LiF single crystals, NaF, MgF_2, silicon). In a single deposition run, thirty circular LiF films with different diameters (4 mm, 10 mm and 18 mm) can be grown on these substrates. The top plate of the vacuum chamber is equipped with an engine, which by rotating the substrate-holder allows obtaining high homogeneity deposition, and with four halogen lamps for heating the substrates [31, 32]. Two water-cooled tantalum crucibles are mounted on the base plate of the chamber, below the substrate-holder at a distance of 22 cm from it. Without opening the vacuum chamber, they can be heated one after the other when two-layered samples need to be deposited. Figure 3 shows the GP20 deposition system and some details of the evaporation chamber.

The evaporation process is performed under a vacuum pressure inside the chamber lower than 1 mPa, obtained by means of a rotary and a water-cooled turbo pumping systems. The film thickness and the evaporation rate are monitored in situ by an INFICON crystal sensor, a fundamental part of the INFICON XTC/2 deposition controller, which uses the Quartz Crystal Deposition Monitor Technique based on the piezoelectric effect [33]. An automatic mechanical shutter is placed over the crucible in order to protect the substrates during the powder pre-heating treatments and to stop the vapour flux, and hence the film growth, when the selected final thickness is achieved. Figure 4 shows thermally evaporated LiF thin films grown on glass and on Si(100) substrates.

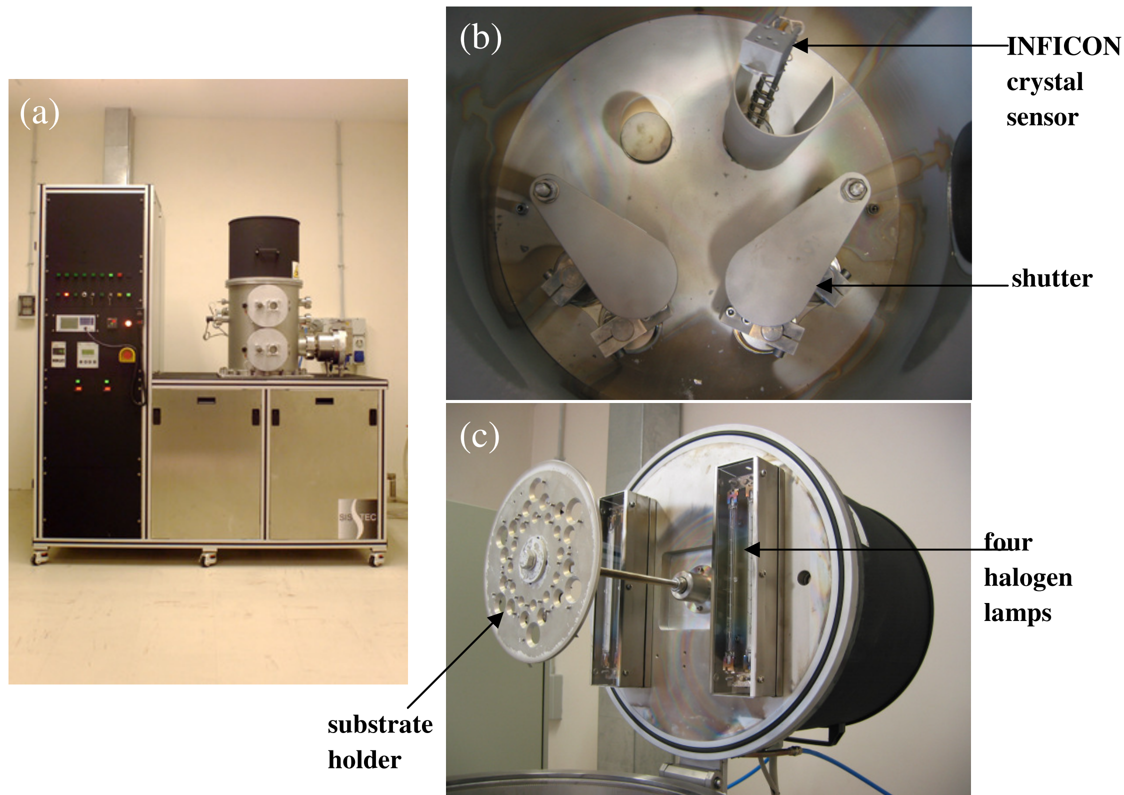

Figure 3. GP20 deposition system (a); inside of the deposition chamber: the shutter and the INFICON crystal sensor are highlighted (b); top cover of the evaporation chamber: the substrate-holder and the four halogen lamps for substrate heating are visible (c).

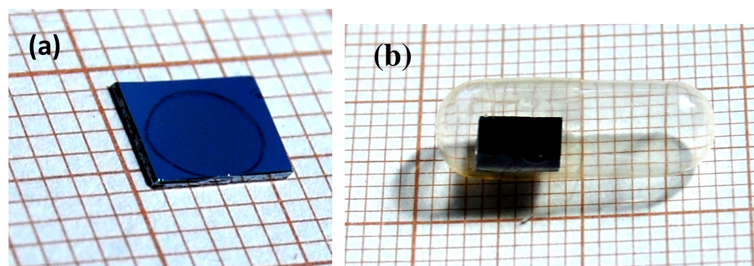

Figure 4. Photograph of a 1.7 μm thick LiF film thermally evaporated on a glass substrate (a) and a (5x5) mm^2 Si substrate (b) inside a plastic transparent box.

5. ATOMIC FORCE MICROSCOPY AND SCANNING ELECTRON MICROSCOPY INVESTIGATION OF LiF THIN FILMS

Several LiF thin films of thickness between 1.0 and 1.6 µm were grown by thermal evaporation on microscope glass slides as substrates, kept at temperatures between 30 °C and 300 °C during the growth, by means of the GP20 deposition system. These substrates were cleaned by using detergents in conjunction with ultrasonic agitation to assure the good adhesion of the film to the substrate.

The starting material consisted of LiF microcrystalline powder (Merck Suprapur, 99.99% pure), heated at about 848 °C in a tantalum crucible. The evaporation rate, monitored in situ by an INFICON quartz oscillator, was automatically controlled to remain at a fixed value of 1 nm/s during the growth. To ensure high uniformity of LiF films, the sample-holder of the GP20 system was continuosly rotating during each evaporation run, as previously described. The thickness of each deposited LiF film was measured after the growth, by using a Tencor Alpha-Step 200 mechanical profilometer.

The morphological analysis of the LiF films was performed with a PARK System AFM, model XE-150, operating in air in non-contact mode, and with a FEG-SEM LEO 1525 at ENEA C.R. Frascati (UTFUS-COND).

In AFM analysis, surface roughness can be characterised by several different profile height sensitive parameters. The Root Mean Square (*RMS*) Roughness is one of the most widely used parameters to quantify the surface roughness. It can be expressed by

$$RMS = \sqrt{\frac{\sum_i (Z_i - Z_a)^2}{N}}$$

where Z_i is the height at each scanned point along the selected line on the investigated surface, Z_a is the average height of the scanned points and N is the total number of data points. Other useful morphological parameters are the peak-to-valley roughness, *Rpv*, and the arithmetic average roughness, *Ra* [31].

Thermally-evaporated LiF thin films are generally polycrystalline and their structural (degree of crystallinity, preferred orientation, compactness, etc.), morphological and optical properties strongly depend on the nature of the substrate, either amorphous or crystalline, and on the deposition parameters, in particular: the substrate temperature, T_s, the film total thickness and the deposition rate [34]. The film growth conditions, which determine the crystallite dimensions and their preferred orientation, void presence and the surface to volume ratio, influence the formation efficiency of primary and aggregate CCs [35] and the optical response of LiF-film based imaging detectors.

Figures 5 and 6 show the 2D and 3D AFM images of a 1 µm thick LiF film, NLiF51 n°7, grown on a glass substrate kept at 300 °C during the growth, acquired across areas of 5×5 µm^2 and of 2x2 µm^2, respectively.

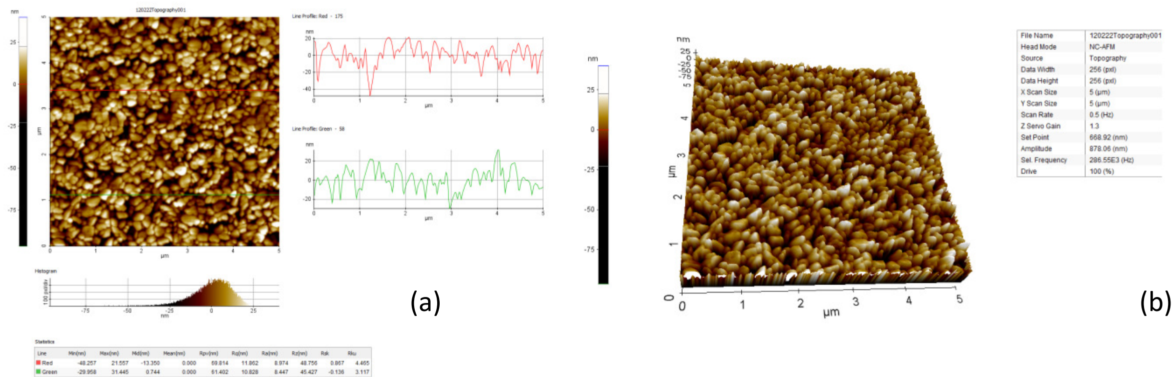

Figure 5. 2D (a) and 3D (b) AFM images of NLiF51 n°7 grown on a glass substrate.

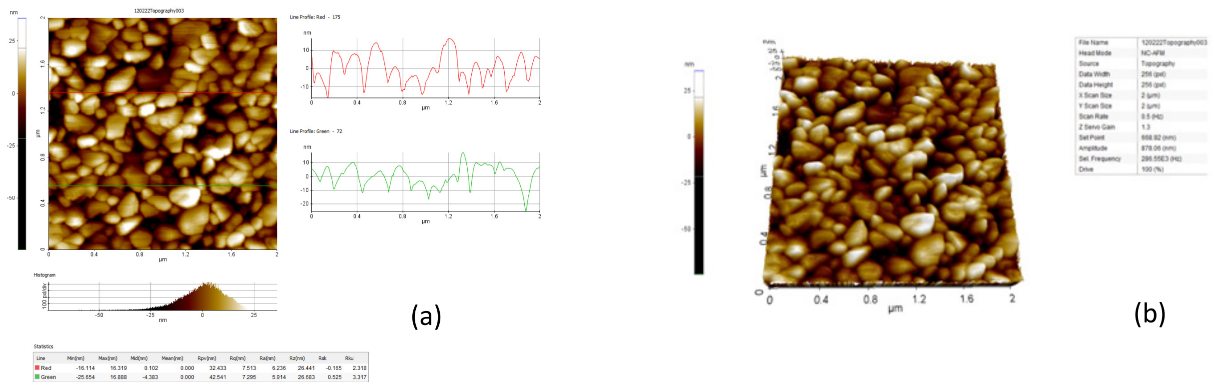

Fig. 6. 2D (a) and 3D (b) AFM images of NLiF51 n°7 grown on a glass substrate.

The morphological parameters of the investigated LiF film, evaluated across an area of 5×5 µm^2, are reported in Table 3.

Table 3. Growth and morphological parameters of NLiF51 n°7.

LiF film	Substrate	T_s (°C)	Thickness (µm)	*Rpv* (nm)	*Ra* (nm)	*RMS* (nm)
NLiF51 n°7	glass	300	1.0	69.814	8.974	11.862
				61.402	8.447	10.828

The morphological analysis allowed to verify the uniformity of the grains, which have a globular and regular shape, and to estimate their dimensions, which are between 50 nm and 250 nm. This evaluation is confirmed by a SEM analysis of the same LiF film, see Fig.7.

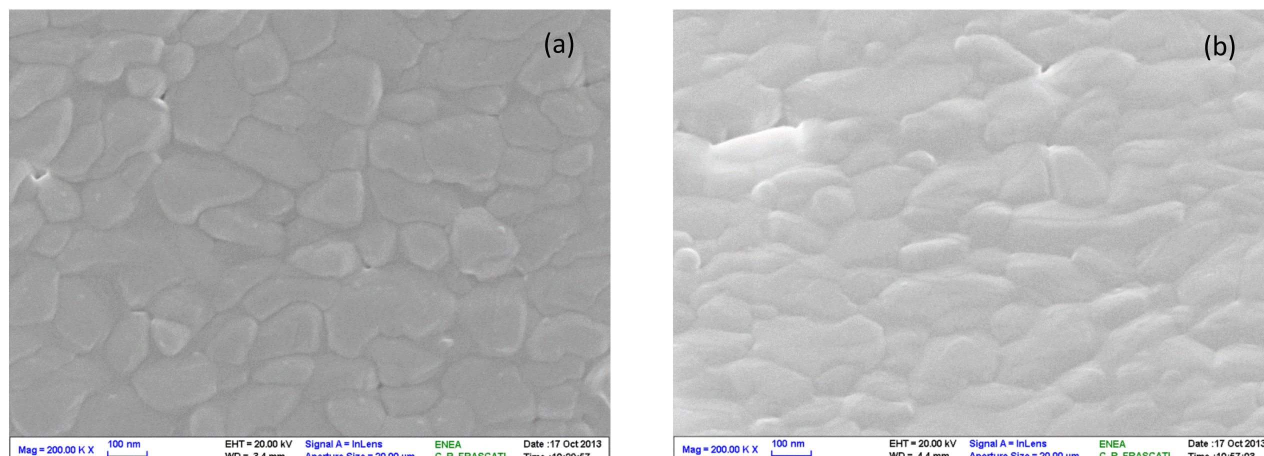

Fig. 7. SEM image of NLiF51 n°7 grown on a glass substrate (a); SEM image of the same sample tilted of 30° (b).

6. SPECTROPHOTOMETRIC CHARACTERISATION OF LiF THIN FILMS

From suitable optical properties of a thin film, like transmittance and reflectance, one can usually estimate a few physical parameters, such as film thickness, surface roughness, material inhomogeneity along the growth axis, refractive index and extinction coefficient spectral behaviour, and so on. This task can be accomplished by means of an instrument able to measure the spectra of the light intensity that is transmitted through (reflected from) the sample being analysed, like a suitably configured spectrophotometer, that in some cases can be equipped with an integrating sphere. These transmittance and reflectance spectra are first measured and later elaborated by adopting a suitable theoretical model for the layer. More in detail, the measured spectra are compared via *ad hoc* developed software with corresponding theoretically computed ones. These latter are modulated by changing proper parameters of the film model until they get as close as possible to the measured spectra – the fitting degree is quantified by a properly defined merit function.

A useful theoretical model should take into account basic and exotic properties of the coating that range, e.g., from its physical thickness and refractive index to density gradients and surface irregularities. To date, a “universal” theoretical model that allows analysing in all respects real-world thin films – layers departing from the ideal model of homogeneous, plane-parallel film on a planar substrate – has not been theorised; however, models have been developed that try and go into that direction by including what are thought to be relevant features – hopefully the most encountered ones – that influence the coating optical response to impinging light. An example of that is a theoretical model that unifies into a single approach three important characteristic [36-38]: material density inhomogeneity along the film growth axis (usually perpendicular to the substrate surface), scattering-scale roughness at the film surface and at its interface with the substrate, and lack of uniformity of the film thickness within the measurement cross section. Recently, this model has been even generalised to the case of a multilayer formed by non-ideal thin films [39].

In the past years, many LiF films on silica substrate were examined in our laboratories following the above mentioned experimental and analytic approach. The LiF films were grown by using the deposition system that is described in sect. 4. The photometric spectral measurements and following analysis were performed in the laboratories of ENEA Casaccia's, UTTMAT-OTT, Rome. The direct transmittance and specular reflectance spectra of the samples were recorded by means of a Perkin Elmer Lambda 900 UV-Vis-NIR spectrophotometer in the wavelength range 190-1600 nm. As far as the reflectance spectra are concerned, they were converted from relative to absolute by using a calibrated reference mirror.

The analysis of the measured spectra was carried out with an *ad hoc* developed Matlab® program that incorporates the recently introduced theoretical model of non-ideal film [36, 37]. Starting from a user-defined selection of film parameters, the program computes synthetic transmittance and reflectance spectra that are quantitatively compared with the corresponding experimental ones by means of a standard chi-square merit function and adjusts the model parameters until the value of the merit function is minimum. The influence of the substrate, which had been previously fully characterised [40], is fully taken into account. The parameter values that give the merit function minimum are the optimal (best fitting) ones for the model. An estimation of their uncertainties is also performed by applying a Montecarlo-like routine that cyclically changes the points of the experimental spectra in a random way, however within the experimental errors, and computes again new values of the model parameters that minimise the new (i.e., calculated with the modified experimental spectra) merit function; the process is repeated a certain number of times – usually from 50 to 100 – until statistics on the model parameters is satisfactory and allows estimating their mean values and standard deviations, which in turn are assumed to be their values and uncertainties [38, 41].

Here we report the spectrophotometric analysis of a LiF film, labelled as NLiF51 n°1, that was deposited over a 1 mm thick Suprasil® silica substrate. This film was grown in the same deposition run with that reported in sect. 5, and should therefore be a replica of it. The approach used for the analysis relies on the best fit of transmittance and reflectance spectra as described above. Nominally, the film was 1 μm thick. During the thermal evaporation, the underlying silica substrate was kept at a constant temperature of ~300 °C. The refractive index and extinction coefficient, n and k, of LiF were assumed to depend on photon energy E according to the following spectral dispersion laws:

$$n(E) = A_0 + \frac{A_1}{E_{0,n}^2 - E^2} \qquad , \qquad k(E) = \frac{k_{\max}}{1 + \left(E - E_{0,k}\right)^2 / \Delta E^2}.$$

Besides the energy E, the quantities appearing in the above formulas are fit parameters.

According to our analysis, the film resulted to be slightly inhomogeneous: its refractive index was found to linearly decrease, in the simplest approximation, from the substrate side to the external medium (air, in our case) side, the gradient (defined as the difference of the extreme index values normalised to their average) being estimated to be $(-1.4 \pm 0.3)\%$. Taking into consideration both the uncertainty on thickness and the thickness inhomogeneity across the measurement cross section (unparallel film faces [36]), the film was found to be on average thick (970 ± 20)nm, with

an air-side *RMS* surface roughness of (17.5 ± 0.2)nm. Note that the roughness found with these optical means is only partially comparable with that found via AFM and reported in Table 3. As a matter of fact, the *RMS* roughness found from optical transmittance and reflectance, and responsible for light scattering, depends on how the probe wavelength compares with the surface autocorrelation length [36-38].

Figure 8 shows the experimental and best fitting theoretical transmittance and reflectance spectra, T and R, plotted against the wavelength $\lambda = \mathrm{hc}/\mathrm{E}$ in the examined spectral range (h and c are Planck's constant and light velocity in vacuum, respectively). Spectra of the bare silica substrate taken before the deposition are also shown in the same figure. The resulting spectral dispersions of this LiF film refractive index and extinction coefficient, n and k, are shown in Fig. 9; since the film has been found to be inhomogeneous, the shown dispersions are evaluated at a depth corresponding to half the layer thickness and should be suitably increased or decreased at any other considered depth. In the left part of Fig. 9, the tabulated dispersion of bulk LiF is also plotted to compare it with the film curve. One can notice how bulk LiF has a higher refractive index than the film one (at half depth, however) in the full examined range. This fact is not surprising as very often, for various reasons (presence of voids among film grains, etc.), solid-state thin films are less compact than the corresponding bulk version of the same material. In the present case, by applying the Maxwell-Garnett effective medium approximation [38] to the tabulated bulk LiF index, we found that the theoretical refractive index of Fig. 9-left is approximately recovered once the density (at half depth) of the examined LiF film is assumed to be ~93% of that of a LiF crystal. Because of the above-discussed density gradient of the refractive index, equal to $(-1.4 \pm 0.3)\%$, one can verify that the LiF film density should approximately linearly decrease from a value of ~95% near the substrate to a value of ~91% in proximity of the external medium (air).

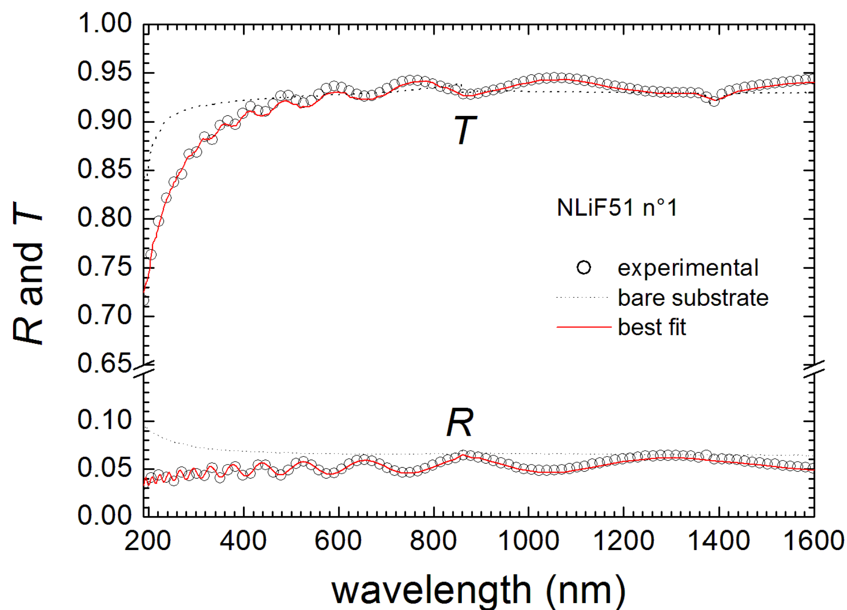

Figure 8. Transmittance and reflectance spectra of sample NLiF51 n°1. Experimental and best fitting theoretical spectra are shown. Measured spectra of the bare silica substrate are also reported.

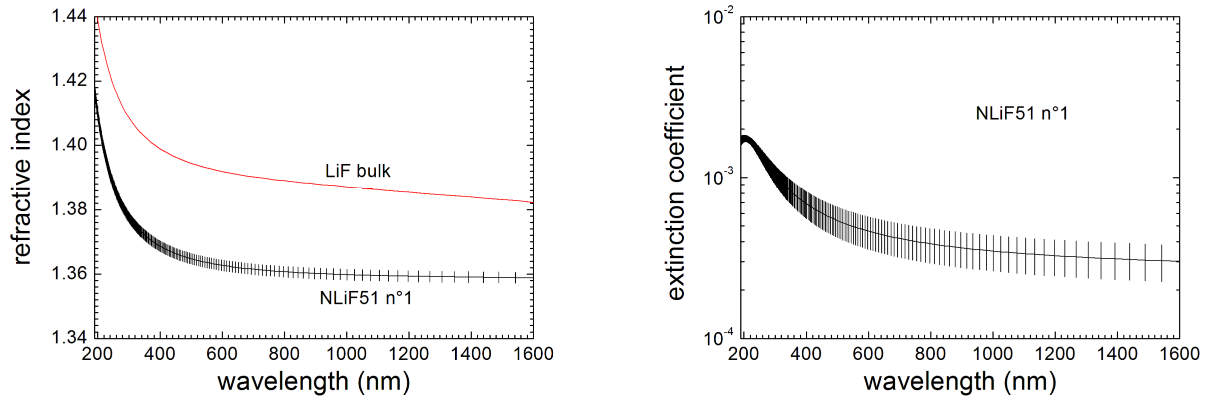

Figure 9. Refractive index (left) and extinction coefficient (right) spectral dispersions of NLiF51 n°1 as found at half depth from the best fit process. The vertical bars indicate the uncertainty band of each curve. In the left figure, the tabulated refractive index of LiF bulk [38] is also plotted.

7. X-RAY DIFFRACTION OF LiF THIN FILMS

LiF thin films grown by thermal evaporation on glass substrates were analysed by means of X-Ray Diffraction, using the Cu K_{α} radiation ($\lambda \cong 0.154$ nm), in order to understand the role of the substrate temperature on the film structural properties. The θ-2θ spectra were collected in a Rigaku Geigerflex diffractometer. Figure 10 shows the X-ray Bragg-Brentano diffraction spectra of NLiF51 n°3, thickness = 1 µm, grown on a glass substrate kept at 300 °C during the growth. Figure 11 reports the θ-2θ diffraction patterns of another LiF film, NLiF46 n°18, thickness = 1.4 µm, grown on a glass substrate kept at 35 °C.

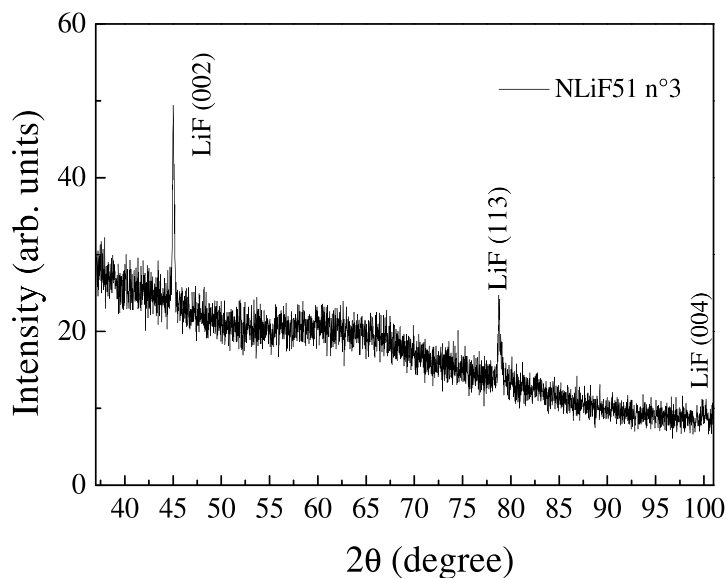

Figure 10. θ-2θ diffraction patterns of NLiF51 n°3, thickness = 1 µm, grown on a glass substrate kept at 300 °C.

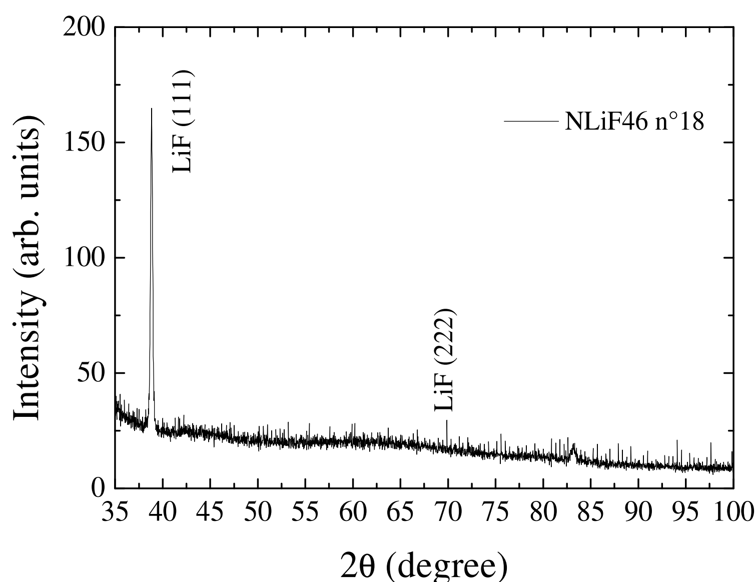

Figure 11. θ-2θ diffraction patterns of NLiF46 n°18, thickness = 1.4 μm, grown on a glass substrate kept at 35 °C.

LiF films thermally evaporated on glass substrates exhibit different preferred orientations depending on the substrate temperature. At high substrate temperature (Ts > 250 °C) a preferred crystalline orientation with the (100) plane parallel to the substrate surface is evidenced by the presence of the more intense (002) LiF reflection in the XRD spectrum of Fig. 10. On the contrary, at lower substrate temperature (see Fig. 11) the crystallites are arranged with their (111) planes almost perpendicular to the substrate surface [24, 35, 42]. Further studies are in progress on this topic.

8. OPTICAL AND SPECTROSCOPIC CHARACTERISATION OF LiF THIN FILMS IRRADIATED BY HIGH-ENERGY ELECTRONS

LiF thin films were coloured at the Radiation Sources Laboratory (UTAPRAD-SOR) of ENEA C.R. Frascati by using high-energy electrons supplied by the LINear ACcelerator, LINAC, which generates square pulses of 4 μs duration and repetition rate from 1 to 280 Hz [43, 44]. The characteristics of the electron beam during the irradiations at RT were: accelerated electron current $I_a = 160$ mA, beam energy $E_e = 5$ MeV (± 2.5%), average dose = 1.26 krad/pulse and repetition rate $\nu = 10$ Hz. At this beam energy, the penetration depth of electrons in LiF is of some millimetres [11].

8.1 Optical absorption measurements of beta-irradiated LiF thin films grown on glass substrates

LiF films of several thicknesses grown by thermal evaporation on glass substrates were irradiated in air at a dose of 8.4×10^4 Gy by means of the electron beam. Optical transmittance spectra in the wavelength range $190 \leq \lambda \leq 1400$ nm were measured with a Perkin Elmer Lambda 950 UV-Vis-

NIR spectrophotometer before and after irradiation. Figure 12 shows the transmittance spectra of a 1.1 µm thick LiF film, NLiF45 n°12, grown on a 1 mm thick glass substrate kept at 300°C during the growth, measured before and after beta irradiation at 8.4×10^4 Gy. The transmittance spectrum before irradiation shows interference fringes due to the refractive index difference between film (~1.39) and substrate (~1.55) [29, 45]. The transmittance spectrum after irradiation changes with respect to the spectrum measured before irradiation because of the formation of CCs in both LiF film and glass substrate.

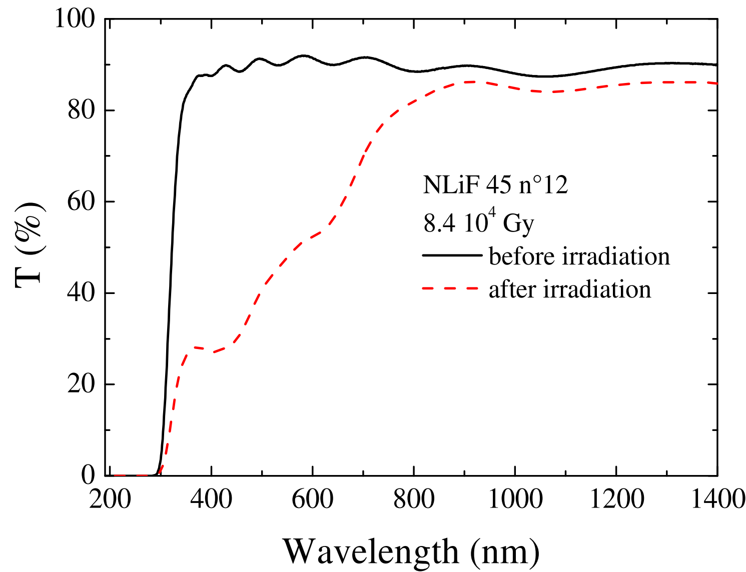

Figure 12. Transmittance spectra of a 1.1 µm thick LiF film, NLiF45 n°12, grown on a glass substrate before and after beta irradiation at 8.4×10^4 Gy.

From a comparison with Fig. 13, which reports the transmittance spectra of an uncoated bare glass substrate measured before and after beta irradiation at the same dose, it is evident that the strong decrease of transmission values at visible wavelengths is almost totally due to the colouration of the 1 mm thick glass substrate.

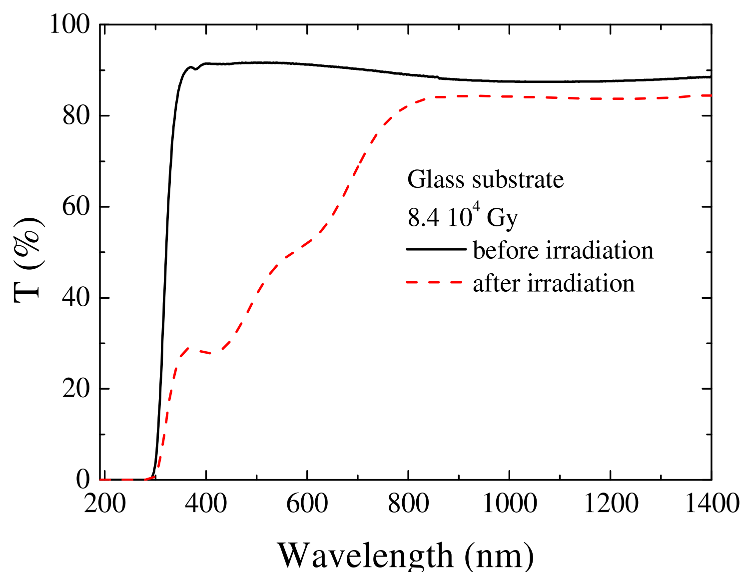

Figure 13. Transmittance spectra of a 1 mm thick glass substrate before and after beta irradiation at 8.4×10^4 Gy.

The colouration of the substrate after beta irradiation is also observable to the naked eye. As shown in Fig. 14, the glass substrate, transparent before irradiation, becomes brown after irradiation.

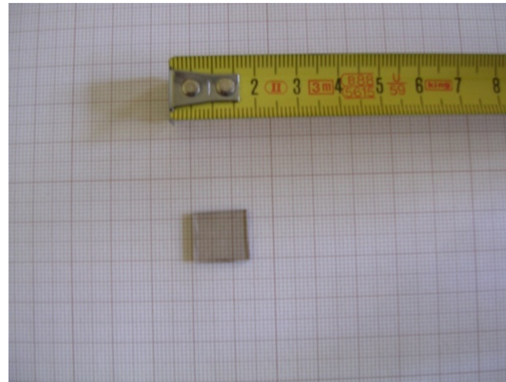

Figure 14. Photograph of a 1 mm thick glass substrate after beta irradiation at 8.4×10^4 Gy.

8.2 *Photoluminescence and photoluminescence-excitation measurements of beta-irradiated LiF thin films grown on glass substrates*

PL and photoluminescence-excitation (PLE) spectra were acquired at RT by means of a Jobin Yvon Fluorolog-3 spectrofluorimeter adopting a front-face detecting geometry. Figure 15 shows the PL spectra of the beta-irradiated LiF thin film, NLiF45 n°12, excited in the M absorption band at the excitation wavelengths, λ_{exc}, of 445 nm and 460 nm. As reported in Table 2, each spectrum consists of two broad emission bands peaked at about 541 nm and 678 nm, due to F_3^+ and F_2 CCs, respectively.

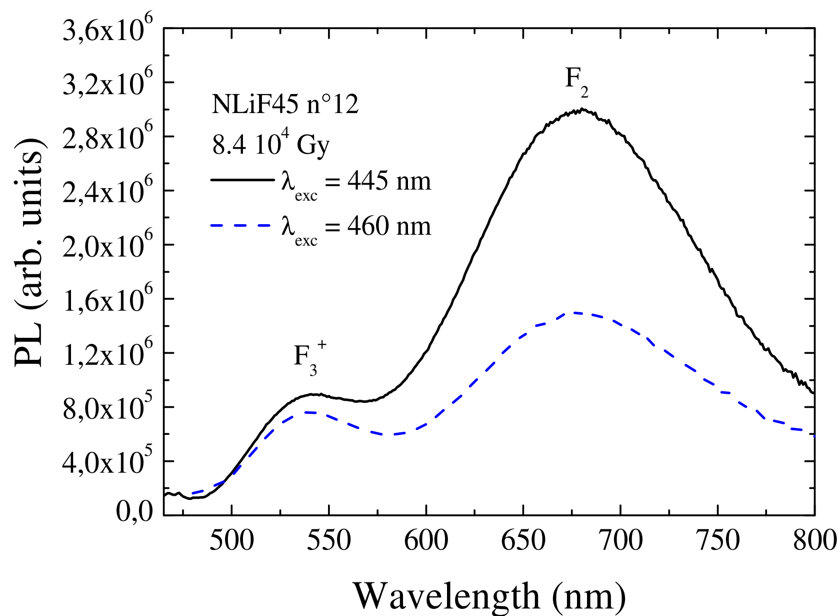

Figure 15. PL spectra of a 1.1 μm thick LiF film, NLiF45 n°12 after beta irradiation at 8.4×10^4 Gy, excited at 445 nm and 460 nm.

Figures 16 and 17 report the PLE spectra of NLiF45 n°12 and of the glass substrate measured after beta irradiation at the same dose and collected at the emission wavelengths, λ_{emi}, of 541 nm and 680 nm, respectively. PLE measurements allow to highlight the contribution due to the presence of visible-emitting F_2 and F_3^+ CCs produced in beta-irradiated LiF film, in spite of the colouration induced by beta irradiation in the glass substrate, whose contribution to visible fluorescence emission is negligible in the investigated measurement conditions.

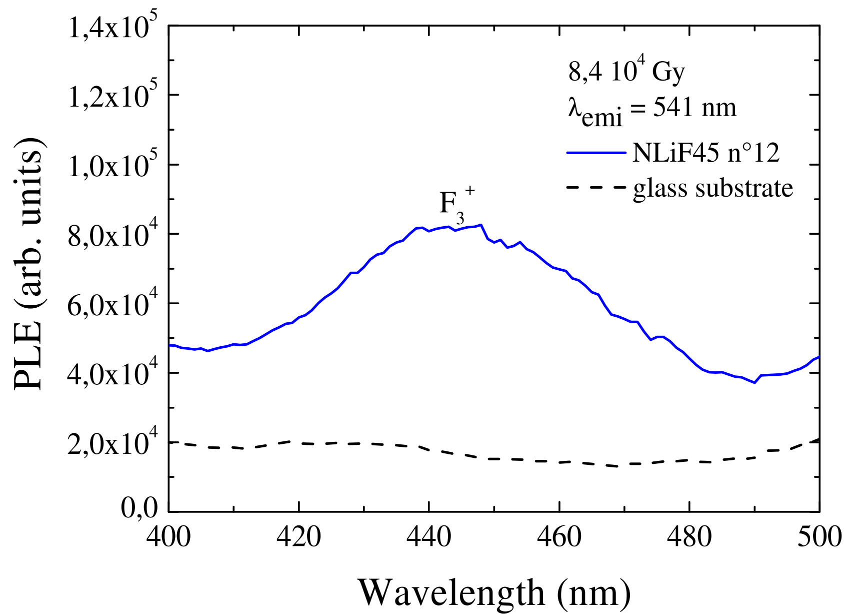

Figure 16. PLE spectra, collected at 541 nm, of a 1.1 μm thick LiF film, NLiF45 n°12, and the glass substrate after beta irradiation at 8.4×10⁴ Gy.

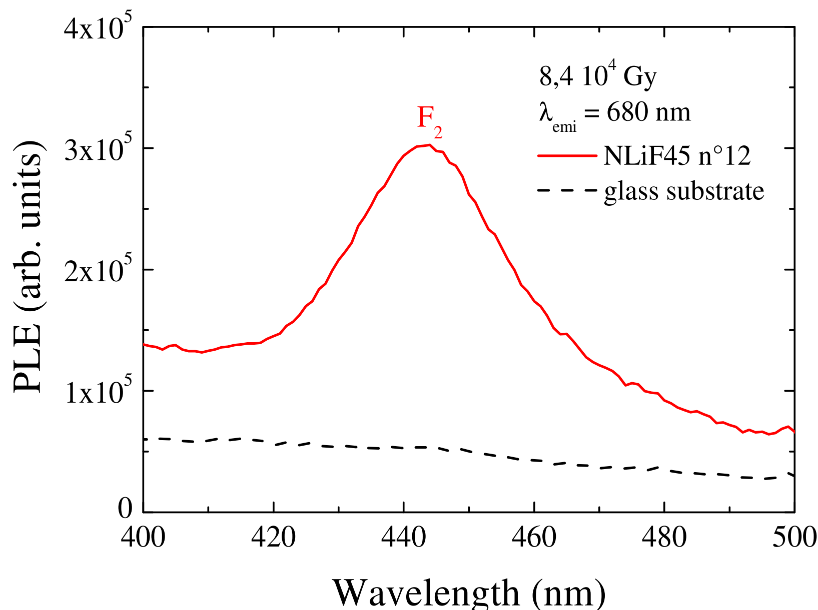

Figure 17. PLE spectra, collected at 680 nm, of a 1.1 μm thick LiF film, NLiF45 n°12, and the glass substrate after beta irradiation at 8.4×10⁴ Gy.

According to the spectral features reported in Table 2, the PLE spectrum at the emission wavelength of 541 nm is broader than that collected at 680 nm. Moreover, its peak position is located at a slightly longer wavelength.

As shown in Table 4, other three LiF films of increasing thickness, grown on glass substrate, were irradiated by the high-energy electrons at the same irradiation dose of 8.4×10^4 Gy.

Table 4. Irradiation dose and thickness of three beta-irradiated LiF films.

Film	T_s (°C)	thickness (μm)	Dose (Gy)
NLiF22 n°3	260	1.1	8.4×10^4
NLiF35 n°7	300	1.3	8.4×10^4
NLiF34 n°2	300	1.6	8.4×10^4

Figure 18 reports the PL spectra of these beta-irradiated LiF films, excited in the M band at 445 nm.

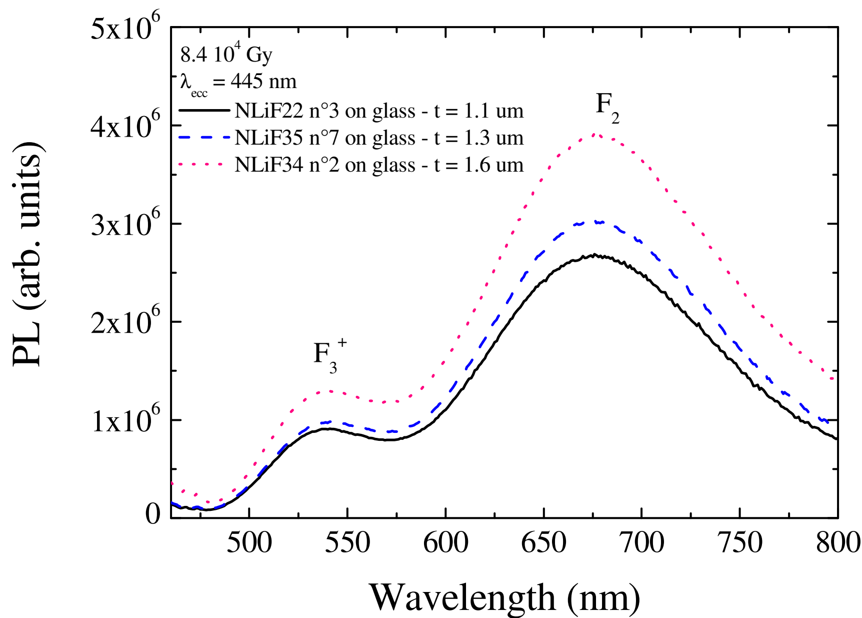

Figure 18. PL spectra of the beta-irradiated LiF films of increasing thickness, excited at 445 nm.

At this electron beam energy, the penetration depth of electrons in LiF is of some millimetres [11] and the LiF films are homogeneously coloured throughout their entire thickness. As shown in Fig. 19, at the same irradiation dose, the F_2 and F_3^+ PL peak intensities at 680 nm and 541 nm, respectively, increase linearly with the film thickness.

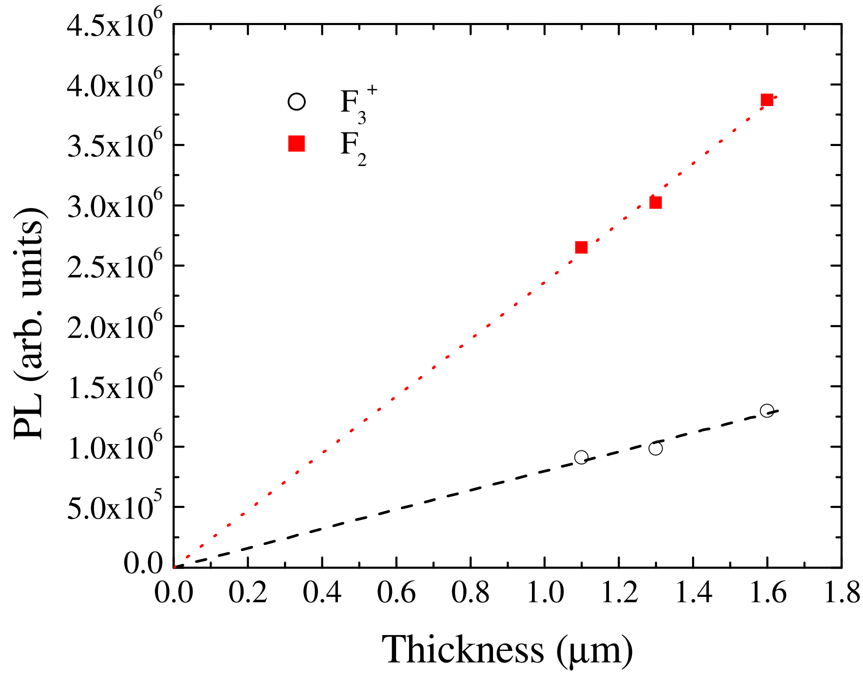

Figure 19. F_2 and F_3^+ PL peak intensities as functions of the LiF film thickness and their linear best-fit.

8.3 Combined Excitation-Emission Spectroscopy

One of the crucial characterisation problems concerning irradiated LiF crystals and films is the coexistence of several kinds of aggregate defects with often overlapping spectral features, which makes it difficult to clearly separate and measure the single contributions of individual CCs (see Table 2). Moreover, in irradiated thin films the direct use of optical absorption spectra to individuate the presence of different kinds of electronic defects is often precluded by the presence of interference fringes due to the refractive index difference between film and substrate (see Fig. 12) [45]. PL measurements are more sensitive than absorption ones to investigate the presence of visible-emitting electronic defects. Performing a complete spectroscopic characterisation by using conventional optical emission and excitation spectroscopy requires a lot of time and guessing, but recently a very effective investigation method, called Combined Excitation-Emission Spectroscopy (CEES) [46, 47], has been developed. In the CEES approach a large number of excitation (or emission) spectra are recorded at a sequence of emission (or excitation) wavelengths. These measurements are used to obtain a three-dimensional graph which shows the excitation intensities as a function of excitation and emission wavelengths. The resulting 3D data set of excitation intensities as a function of excitation and emission wavelengths can be best visualized in a contour plot, where lines of equal emission intensity are drawn. In this data rappresentation, a single emission band excited in a single absorption band appears, similarly to a geographic map, as a mountain, while the asymmetries of the observed peaks allow to distinguish the spectral contributions of different states in the same optical range.

PLE spectra of the sample NLiF45 n°12 (see Figs.16, 17), beta-irradiated at a dose of 8.4×10^4 Gy, were collected shifting the emission wavelength by 5 nm after each acquisition in the spectral interval extending from 430 nm to 800 nm, where the F_2 and F_3^+ emission bands are located. All

the collected PLE spectra are shown in the 3D and 2D graphs shown in Fig. 20, where the resulting data set of excitation intensities as a function of excitation and emission wavelengths is visualised. This kind of representation gives a global view of all the emission and excitation peaks and allows to distinguish each emission band and correlate it to the appropriate excitation wavelengths.

Figure 20 shows only two peaks, due to F_2 and F_3^+ CCs, at excitation wavelengths around 450 nm, in agreement with the selected spectra reported in Figs. 16 and 17. The intensity scale allows to unambiguously identify them in the 2D projection in the λ_{emi}, λ_{exc} plane (Fig. 20 b). In spite of the high beta irradiation dose of the investigated LiF film, the contributions due to more complex CCs are not observed. A similar result was obtained studing gamma-irradiated LiF thin films at doses up to 10^6 Gy by CEES technique [48]. On the contrary, the investigation of a beta-irradiated LiF crystal at the same dose (8.4×10^4 Gy) has shown the presence of F_3 CCs [49].

This approach is very suitable for the investigations of coloured thin films, as it is possible to neglect the effects of the sample optical absorption [50] at the used excitation wavelengths and to use directly their PLE spectra as acquired. On the contrary, the effect of the sample optical absorption is significant in coloured LiF crystals [51], because of their higher thickness.

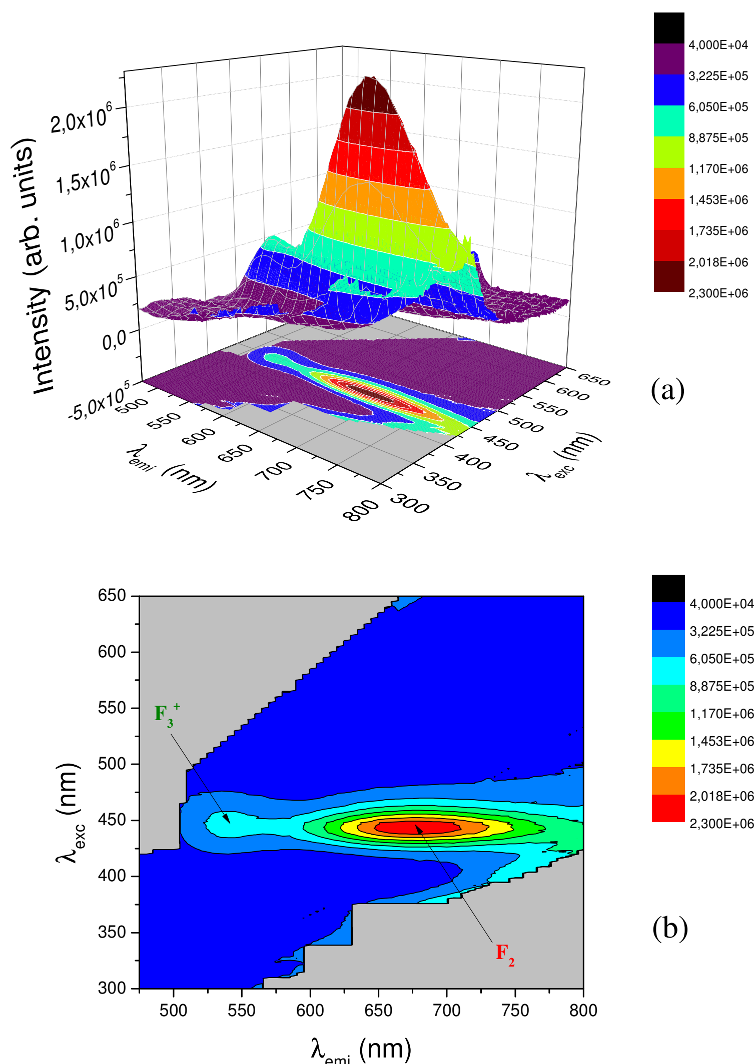

Figure 20. 3D (a) and 2D (b) representations of the PLE spectra of a 1.1 μm thick LiF film, NLiF45 n°12, after beta irradiation at 8.4×10⁴ Gy collected at RT.

CONCLUSIONS

Polycrystalline LiF thin films, about 1 μm thick, deposited by thermal evaporation on glass substrates in controlled growth conditions, were characterised by means of AFM, SEM and XRD techniques. Starting from optical transmittance and reflectance spectra, a theoretical model was used to evaluate thickness, refractive index, surface roughness and material inhomogeneity along the growth axis of a LiF thin film. Optical absorption, photoluminescence and photo-excitation spectra of LiF thin films of increasing thicknesses were measured before and after irradiation with high-energy electrons at a dose of 8.4×10^4 Gy. An advanced spectroscopic characterisation, called Combined Excitation-Emission Spectroscopy, has been performed for the first time on a beta-irradiated LiF film grown on glass. The information obtained by using the CEES technique could have been derived from conventional systematic PLE spectra, but the CEES approach makes it easier and effective to isolate the different spectral contributions buried in the broad absorption and emission bands peaking in the visible range. This approach is very suitable for the investigation of low-absorbing, efficient light-emitting thin films, like beta-coloured LiF films, in order to individuate correlations between the CC stable formation and growth conditions.

In spite of the high beta irradiation dose of the studied LiF films, PL contributions due to CCs more complex than the F_2 and F_3^+ defects were not detected in the investigated spectral range.

The presented results are in agreement with previous literature and make the use of LiF films as fluorescent detectors for high-energy electrons a reliable tool.

REFERENCES

[1] *Handbook of Chemistry and Physics*, 78th Ed., CRC Press Inc., Cleveland, Ohio, 1997-98.

[2] M. Piacentini, *Solid State Commun*. 17, 697 (1975).

[3] *Handbook of Optical Constants of Solids*, Palik E.D., Ed., Academic Press, New York (1985).

[4] A.T. Davidson, A.G. Kozakiewicz, D.J. Wilkinson, J.D. Comins, *J. Appl. Phys.* 86, 1410 (1999).

[5] G. Baldacchini, R.M. Montereali, E. Nichelatti, V.S. Kalinov, A.P. Voitovich, A.T. Davidson, A.G. Kozakiewicz, *J. Appl. Phys.* 104, 063712-1-10 (2008).

[6] V.V. Ter-Mikirtychev, T.T. Tsuboi, *Prog. Quantum Electr.* 20 (3), 219 (1996).

[7] R.M. Montereali, M. Piccinini, E. Burattini, *Appl. Phys. Lett.*78 (26), 4082 (2001).

[8] W.B. Fowler, *Physics of Color Centers*, W.B. Fowler, New York and London: Academic Press Inc (1968).

[9] S.W.S. McKeever, M. Moscovitch, P.D. Townsend, *Thermoluminescence Dosimetry Materials: properties and uses*, Nuclear Technology Publishing, Ashford, Kent TN23 1YW, England (1995).

[10] G. Diambrini-Palazzi, *Introduzione a problemi di frontiera della fisica subnucleare*, ARACNE (1997).

[11] G. Baldacchini, E. Ciaramella, G. Messina, R.M. Montereali, *ENEA Technical Report* RT/INN/91/54 (1991).

[12] W. Gellermann, *J. Phys. Chem. Solids* 52 (1), 249 (1991).

[13] J.H. Crawford, *Adv. Phys.* 17, 93 (1968).

[14] J. Nahum, D.A. Wiegand, *Phys. Rev.* 154, 817 (1967).

[15] E. Hughes, D. Pooley, H.U. Rahman and W.A. Runciman, *Harwell Atomic Research Establishment* R-5604 (1967).

[16] F. Seitz, *Rev. Mod. Phys.* 26, 7 (1954).

[17] G. Baldacchini, M. Cremona, U.M. Grassano, V. Kalinov and R.M. Montereali, in *Defects in Insulating Materials* (O. Kanert and J.M. Spaeth, Eds.), World Scientific, Singapore (1993), 1103-06.

[18] E. Sonder and W.A. Sibley, *Point Defects in Solids* (J.H. Crawford and L.M. Slifkin, Eds.), Chap. 4, Plenim Press, New York (1972).

[19] J. Nahum, *Phys. Rev.* 158, 814 (1967).

[20] A. Perez, J. Davenas and C.H.S. Dupuy, *Nucl. Instrum. Methods* 132, 219 (1976).

[21] M. Montecchi, E. Nichelatti, A. Mancini and R.M. Montereali, *J. Appl. Phys.* 86 (7), 3745 (1999).

[22] V.V. Ter-Mikirtychev and T.T. Tsuboi, *Canad. J. Phys.* 75, 813 (1997).

[23] G. Baldacchini, E. De Nicola, R.M. Montereali, A. Scacco, V. Kalinov, *J. Phys. Chem. Solids* 61, 21 (2000).

[24] R.M. Montereali, G. Baldacchini, S. Martelli, L.C. Scavarda do Carmo, *Thin Solid Films* 196, 75-83 (1991).

[25] R.A. Nunes, A.P. da Silva Sotero, L.C. Scavarda do Carmo, M. Cremona, R.M. Montereali, M. Rossi, F. Somma, *J. Luminescence* 60-61, 552 (1994).

[26] A. Perea, J. Gonzalo, C.N. Afonso, S. Martelli, R. M. Montereali, *Appl. Surf. Sci.* 138-139, 533 (1999).

[27] B.A. Movchan and A.V. Demchishin, *Phys. Met. Metallogr.* 28, 83-91 (1969).

[28] P.B. Barna, M. Adamik, *Thin Solid Films* 317, 27-33 (1998).

[29] K.D. Leaver, B.N. Chapman, *Thin Films*, Wykeham Publications (London) LTD, London and Winchester (1971).

[30] J. Venables, *Introduction to Surface and Thin Film Processes*, Cambrige U. Press, Cambrige, UK (2000).

[31] S. Gambino, G. Baldacchini, I. Franzini, R.M. Montereali, M.A. Vincenti, V. Mussi, *ENEA Technical Report*, RT/2006/68/FIM (2006).

[32] SISTEC, Heating boat evaporation deposition system GP20/n°10352, *Installation, use and maintenance handbook* (2004).

[33] Leybold INFICON, *XTC/C and XTC/2 Operating manual* (1997).

[34] R.M. Montereali, *Handbook of Thin Films Materials*, Academic Press, Vol. 3, Cap. 7 (2002), and references there in.

[35] G. Baldacchini, M. Cremona, G. d'Auria, S. Martelli, R.M. Montereali, M. Montecchi, E. Burattini, A. Grilli, A. Raco, Nucl. Inst. Meth. B 116, 447-451 (1996).

[36] M. Montecchi, R.M. Montereali, and E. Nichelatti, *Thin Solid Films* 396, 262 (2001).

[37] M. Montecchi, R.M. Montereali, and E. Nichelatti, *Thin Solid Films* 402, 311 (2002).

[38] E. Nichelatti, M. Montecchi, R.M. Montereali, *Thin Solid Films* 515, 4640 (2007).

[39] E. Nichelatti, M. Montecchi, R.M. Montereali, *J. Non-Cryst. Solids* 355, 1115 (2009).

[40] E. Nichelatti, *J. Opt. A: Pure Appl. Opt*. 4, 400 (2002).

[41] E. Nichelatti, F. Bonfigli, A.Ya. Faenov, F. Flora, T. Marolo, M. Montecchi, R.M. Montereali, T. Pikuz, G. Baldacchini, J. *Non-Crystalline Solids* 351, 1774 (2005).

[42] P.E. Di Nunzio, L. Fornarini, S. Martelli, and R.M. Montereali, *phys. stat. sol. (a)* 164, 747–756 (1997).

[43] U. Bizzarri, G. Messina, A. Vignati, *Rapporto Tecnico ENEA* P2/43 (1982).

[44] L. Picardi, C. Ronsivalle, *Rapporto Tecnico ENEA*, RTI/TIB/87-38 (1987).

[45] E. Nichelatti, R.M. Montereali, M. Montecchi, T. Marolo, *J. Non-Crystalline Solids* 322, 117-121 (2003).

[46] D.M. Gill, J.C. Wright, L. McCaughan, *Appl. Phys. Lett.* 64 (19), 2483-2485 (1994).

[47] V. Dierolf, A.B. Ktsennko, C. Sandmann, Th. Troster, G. Corradi, *J. Lumin.* 87-89, 989-991 (2000).

[48] M.A. Vincenti, T. Marolo and R.M. Montereali, *Radiation Measurements* 45, 359–361 (2010).

[49] M.A. Vincenti, *Lithium fluoride: a promising material for versatile radiation detectors*, PhD Thesis (2012).

[50] L. Skuja, *Defects in SiO_2 and Related Dielectrics: Science e Technology*, Edited by G. Pacchioni, L. Skuja, D. L. Griscom, NATO Science Series, 73-116 (2000).

[51] T. Marolo, G. Baldacchini, V.S. Kalinov, R.M. Montereali, *phys. stat. sol. (c)* 2, No. 1, 367-370 (2005).

Edito dall' ENEA
Servizio Comunicazione

Lungotevere Thaon di Revel, 76 - 00196 Roma

www.enea.it

Stampa: Tecnografico ENEA - CR Frascati
Pervenuto il 9.12.2013
Finito di stampare nel mese di gennaio 2014